The Ultraviolet Environment of a Tropical Megacity in Transition: Mexico City 2000-2019

Adriana Ipiña,[*,†,‡] Gamaliel López-Padilla,[¶] Armando Retama,[§] Rubén D. Piacentini,[†] and Sasha Madronich[‖]

[†]*Instituto de Física Rosario (CONICET-UNR), Rosario, Argentina*

[‡]*Centro de Ciencias de la Atmósfera, Universidad Nacional Autónoma de México, Mexico City, Mexico*

[¶]*Facultad de Ciencias Físico Matemáticas, Universidad Autónoma de Nuevo León, San Nicolás de los Garza, México*

[§]*Independent researcher, Mexico City, Mexico*

[‖]*National Center for Atmospheric Research, Boulder, Colorado, USA*

E-mail: ipina@ifir-conicet.gov.ar

Abstract

Tropical regions experience naturally high levels of UV radiation, but urban pollution can reduce these levels substantially. We analyzed 20 years of measurements of the UV Index (UVI) at several ground-level locations in the Mexico City Metropolitan Area and compared these with UVI values estimated from satellite overpasses observing ozone and clouds (but not local pollution). The ground-based measurements were systematically lower than the satellite-based estimates, by ca. 40% in 2000 and 20% in 2019. Calculations with a radiative transfer model and observed concentrations of air

pollutants explained well the difference between satellite- and ground-based UVI, and showed specific contributions from boundary layer and free trophosperic aerosols, O_3, NO_2, and SO_2, in decreasing order of importance. Such large changes in UV radiation between 2000 and 2019 have important implications ranging from human health (skin cancer and cataract induction) to air pollution control (photochemical smog formation).

Introduction

Ultraviolet (UV) radiation is an important component of the urban environment, affecting human populations directly through UV exposure of skin and eyes[1–3] and less directly (but with great impact) by driving the formation of photochemical smog, including tropospheric ozone and other oxidants, as well as secondary aerosols containing nitrates, sulfates, and organics.[4–6] These pollutants, along with others of primary origin commonly found in urban atmospheres (e.g., black carbon, sulfur dioxide), can in turn scatter and/or absorb UV radiation, alter its vertical distribution, and so modify the photochemical rate of their own formation. Such feedback complicates the calculation of both the UV radiation field (including at the surface), and the evolution of photochemical smog in the urban boundary layer.

The question of how air pollution alters the urban UV environment (and *vice versa*) is not new, but studies have relied mostly on numerical models,[7–9] with relatively fewer available observations (e.g., McKenzie et al.[10], Panicker et al.[11], Palancar et al.[12], reviewed by Bais et al.[13]). Increases in UV have been estimated in association with decadal emission reductions, e.g. in China,[14–16] and that have led to less-than-expected reductions in photochemical smog, in part due to stronger UV photochemistry.[17–19] Emission reductions have also occurred globally during the 2020 COVID-19 pandemic,[20,21] but ground-level ozone in some polluted areas has actually increased,[22,23] due at least in part to the increased UV radiation. Unfortunately, the observational data base of relevant UV radiation remains rather sparse to evaluate such model-derived hypotheses.

The environment of Mexico City is of particular interest for several reasons: (1) Nearly 23 million people inhabit the Mexico City Metropolitan Area (MCMA), and the UV environment has direct implications for their health, both in terms of skin/eye UV exposure and *via* photochemical smog formation. (2) As a tropical megacity, it is to some extent representative of the situation of many others, with year-round intense midday UV irradiance, a shallower atmosphere due to the city's high elevation of 2240 m above sea level, and a transition toward newer and cleaner technologies, leading to gradual improvements in air quality. (3) Air quality within MCMA has undergone extensive scrutiny, with a well-established monitoring network since 1986,[24] numerous intensive field campaigns to study the meteorology, emissions, and photochemistry of smog formation,[25–27] and numerical modeling incorporating the evolving knowledge.[28–31] This extensive body of knowledge provides the foundation for understanding our study.

Here, we analyze two decades of continuous measurements of the UV Index at multiple locations within the MCMA, collected by the Secretariat of the Environment (Secretaría del Medio Ambiente, SEDEMA)[1] of the Mexico City government as part of an intensive monitoring network over the MCMA. The UV Index is defined as:

$$UVI = 40 \int_{250nm}^{400nm} E\left(\lambda, t\right) \cdot S_{er}(\lambda) d\lambda \tag{1}$$

where $E(\lambda, t)$ is the solar spectral irradiance in units of W $\cdot$m^{-2} $\cdot$nm^{-1} and $S_{er}\left(\lambda\right)$ is the erythemal sensitivity of human skin.[32,33] Multiplication by 40 was chosen historically to express the UVI in small integer numbers, but is otherwise scientifically arbitrary.

The UVI is recognized by the World Health and Meteorological Organizations (WHO and WMO) as a standardized metric of UV radiation[32] for global public information. An advantage of using the UVI as (one) metric of UV radiation is that it is being increasingly observed or calculated and disseminated, enabling more objective comparisons among seasons and locations. The UVI observations from Mexico City, considered here, are an important

[1] https://www.sedema.cdmx.gob.mx/

element of this global picture.

While the UVI at the surface cannot be translated directly into photolysis frequencies for various photo-labile molecules, the spectral weighting of the UVI (ca. 300-320 nm) is approximately similar to that for the photolysis of ozone to singlet oxygen atoms. Other UV wavelengths are of course also important, e.g. for the photolysis of nitrogen dioxide, and may be affected differently depending on the pollutant. With these considerations and a few other caveats, UVI trends examined here can also be used to infer accompanying trends in photolysis frequencies and influences on photochemical smog formation.

Methods

Ground-based measurements

The Mexico City Metropolitan Area is located at 19.4°N, 99.1°W, 2240 meters above sea level (asl), surrounded by mountain ridges exceeding 5000 m asl, with complex topography and thermal inversions that inhibit winds and favor intense air pollution.[34–36] Air quality monitoring and surface meteorological measurements in the MCMA are conducted continuously by the Automated Atmospheric Monitoring Network (RAMA, by its Spanish acronym) of the Atmospheric Monitoring System (SIMAT, by its Spanish acronym) of the Mexico City government. Since the year 2000, UV radiometers (model 501-A, Solar Light Company Inc., Glenside, PA) detecting wavelengths between 280-400 nm have been measuring erythemally-weighted solar radiation. The calibration of the UV sensors was carried out annually by comparing against a factory-calibrated reference sensor. The output voltages from the measuring sensors were compared during at least one week against the UV readings from the reference sensor to derive the calibration factor. New calibration factors typically differed from the old ones by 2% or less. Reference sensors were also calibrated by the manufacturer and updated periodically (between 3 to 5 years) to avoid any bias due to aging. Long term calibration drift was avoided by the yearly re-calibrations. Although at the beginning only

a few stations were in operation and have been changing, currently 11 stations are recording erythemal irradiances, which are then multiplied by 40 (see Eq. 1) to give UV Indices. Table 1 describes the location of the stations where UV Index has been measured. Figure 1 shows how the radiometers of the SIMAT have been distributed over MCMA, prioritizing the sites with more density of population. Near real-time data for each station are available on the SIMAT official website http://www.aire.cdmx.gob.mx/default.php. Daily maximum values ($UVI_{\max}$) were extracted from each of the stations around solar noon from the time interval from 11:00 h-15:00 h CST (Central Standard Time). This database with 7305 continuous days of measurements during the period 2000-2019 was analyzed.

Table 1: SIMAT stations and AERONET site*, environmental descriptors and geographical positions. Abbreviations names: Chalco (CHA), Cuautitlán (CUT), FES Acatlán (FAC), Hangares (HAN), Laboratorio de Análisis Ambiental (LAA), Merced (MER), Montecillo (MON), Milpa Alta (MPA), Pedregal (PED), San Agustín (SAG), Santa Fe (SFE), Tlalnepantla (TLA) and National Autonomous University of Mexico (UNAM*)

Station	Environment	Lat (^{o}N)	Lon (^{o}W)	El (masl)
CHO	semi-urban	19.27	98.89	2253
CUT	ecological park	19.72	99.20	2263
FAC	urban	19.48	99.24	2299
HAN	urban	19.42	99.08	2235
LAA	urban	19.48	99.15	2255
MER	downtown	19.42	99.12	2245
MON	rural	19.46	98.90	2252
MPA	rural	19.18	98.99	2594
PED	residential	19.33	99.20	2326
SAG	urban	19.53	99.03	2241
SFE	residential	19.36	99.26	2599
TLA	urban	19.53	99.20	2311
UNAM*	University city	19.33	99.18	2294

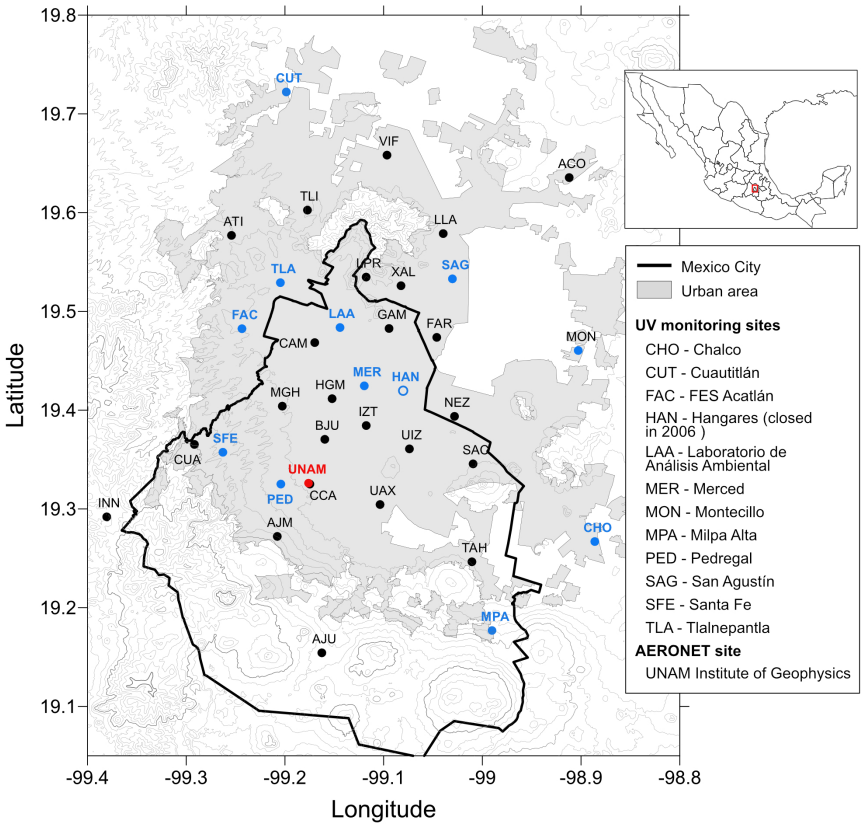

Figure 1: Map with the location of the SIMAT continuous monitoring stations over MCMA. Sites denoted by the blue solid dots correspond to SIMAT stations with UV measurements, while the black dots indicate SIMAT stations without UV measurements, the site on open blue dot represents a discontinued site, the red dot corresponds to the location of the AERONET site. The location of Mexico City and the acronyms of the UV and AERONET site are shown at the upper and lower frames at the right respectively.

With the aim to explore the relationship between UVI and air pollutants levels, the hourly averages for ozone (O_3), carbon monoxide (CO), nitrogen dioxide (NO_2), sulfur dioxide (SO_2) and particle matter with diameter sizes ≤ 10 μm (PM_{10}), were downloaded from the SIMAT.[37] For purposes of assessing the influence on the UV Index at solar noon, only values obtained between 11h and 15h CST were considered for the trends analysis. Pollutant measurements are conducted by the SIMAT using regulatory-grade commercial instruments. Measurement principles include ultraviolet photometry (model 400E, Teledyne-API) for O_3, chemiluminescence (model 200E, Teledyne-API) for NO_2, UV fluorescence (model 100E, Teledyne API) for SO_2, and infrared absorption (model 300E, Teledyne-API) for CO.

The PM_{10} continuous mass concentration was measured with Tapered Element Oscillating Microbalance (TEOM 1400AB or TEOM 1405 DF, Thermo Scientific) monitors. Gaseous pollutant levels are reported in ppb concentration units for O_3, SO_2 and NO_2, and in ppm for CO. Particulate matter mass concentration is reported in μg m^{-3} at local conditions for temperature and pressure.

Aerosol optical depth at 340 nm was obtained from the Institute of Geophysics of the National Autonomous University of Mexico (UNAM); measurements were conducted with a CIMEL sun photometer model CE-318, which is an automatic sun-sky-scanning spectral radiometer of the AErosol RObotic NETwork (AERONET[38]). The data Product Level 2.0 and 1.5 (only in 2019) were selected, and annual averages AOD_{340} were calculated from continuous measurements during at least 7 months. A previous study of the AOD behavior from 2000 to 2014 demonstrated that the gaps of data did not significantly change the trends over the analyzed period.[39] From 2014 to 2019 there was only 8% of the missing data, when the instrument was sent for calibration in 2018.

Satellite data

Estimates of the UV Index from satellite-based measurements of clouds and O_3 were used for comparing to the ground-based measurements. These data were provided by the Ozone Monitoring Instrument (OMI) on board of AURA-NASA satellite.[40] OMI was created in co-operation between the Netherlands Agency for Aerospace Programmes (NIVR), the Finnish Meteorological Institute (FMI) and NASA. OMI (hereafter OMI-Aura/NIVR-FMI-NASA) performs observations over a geographical dimension of $13\times24km^2$ at nadir. For Mexico City, the satellite overpass time is between 19:00h - 21:00h UTC and data are specific for the coordinates and elevation of Mexico City. Measurements of the ozone profile and cloud cover are used via a radiative transfer model to estimate the UVI at the ground. The OMI web site reports UVI values for both the overpass time, and corrected to local solar noon.

While the early OMI estimates of the UVI did not consider aerosols in the boundary

layer, Arola et al.[41] suggested correcting the clean-skies UV index with a reduction factor based on a monthly global climatology of BL aerosols. For Mexico City a reduction of about 8% is applied, starting ca. 2013, to the OMI UVI data.

TUV model

Calculations of the UV Index were also made with the Tropospheric Ultraviolet Visible (TUV v5.3) model.[42] The model atmosphere was represented by 80 vertical layers, each 1 km thick, starting at the 2.24 km asl elevation of MCMA, and for which the first three km constitute the atmospheric boundary layer (BL).[43] The ozone profile above the BL is from the US Standard Atmosphere, but rescaled to a value of 259.6 DU. Totals including the BL contributions (of 13.7 DU in the year 2000 and 9.8 DU in 2019, see below) were 273.1 DU in 2000 and 269.2 DU. The climatological O_3 column for this latitude and season is about 270 DU (plus or minus ca. 5 DU) so in good agreement with the values used here.

Pollutants within the BL (including O_3) are assumed to be well mixed, in agreement with observations from the MILAGRO field campaign that showed the disappearance of vertical gradients in the profiles of gases[44,45] and aerosols[46,47] by late morning. The UV-absorbing gases considered here are O_3, NO_2, and SO_2, specified in ppb.

BL aerosols are modeled by prescribing the AOD at 340 nm (from AERONET observations), scaled to other wavelengths inversely with wavelength (Angstrom coefficient = 1.0), asymmetry factor of 0.7, and a single scattering albedo of 0.85 at UV wavelengths, following the determinations made in Mexico City by Corr et al.[48] and Palancar et al.[12].

Above the atmospheric boundary layer, the model was taken to be free of aerosols, NO_2, or SO_2. In one sensitivity study, a total AOD of 0.7 was redistributed placing 0.2 in the free troposphere (decreasing vertically with an exponential scale height of 4 km, and 0.5 remaining in the BL). The calculated UVI differed by less than 1%. Thus, as long as the total AOD is known, knowledge of the exact vertical aerosol profile is not critical towards ground-level UVI – but would obviously affect the vertical structure of photolysis frequencies.

Radiative transfer calculations were carried out with the pseudo-spherical 4-stream option, at 1 nm steps between 280 and 400 nm.

Results and Discussion

Figure 2 shows the diurnal variation of the UVI for several specific cloud-free days, for different seasons and several locations (CHO, MER, MON, PED, SAG, SFE and TLA). UV Index from TUV model was used as reference of the behavior under clear sky days. According to the comparison of measurements minute by minute, the dates with prolonged fluctuations along the day were discarded. However, during the rainy period (from June to October) at least a brief clouds presence is common, as shown at CHO station around noon in 13 June 2017. Peak values range from 8 during autumn/winter to above 12 in spring/summer, in correspondence to the respective December and June solstices. Although the stations are all within a 25 km radius, substantial differences among them are notable. Survey of the locations revealed that shadowing from nearby structures is not an issue. The good agreement in the morning, followed by more divergence in the afternoon, is consistent with the development of photo-chemical pollution hotspots during the day. Previous studies (e.g., Castro et al.[49] and Palancar et al.[12]) have shown that surface UV radiation in Mexico City is attenuated significantly by aerosols. The measurements shown in Fig. 2 are consistent with this increasing pollution during the course of the day, with highest aerosol loading (and highest variability) attained in the afternoon. Further support for the role of pollution in suppressing the UVI comes from the observation made at the Santa Fe (SFE) site which in Fig. 2 are seen to be systematically higher, e.g. by over 10% in autumn afternoons, compared to the other stations. The SFE station is displaced to the west from the majority of the other stations, and remains in the outskirts. This site is also approximately 300 m higher than Mexico City downtown, so that the cleaner atmosphere results from both vertical and horizontal variations in pollution levels.[50] It is indeed expected to have higher values of the

UVI, in agreement with the observations.

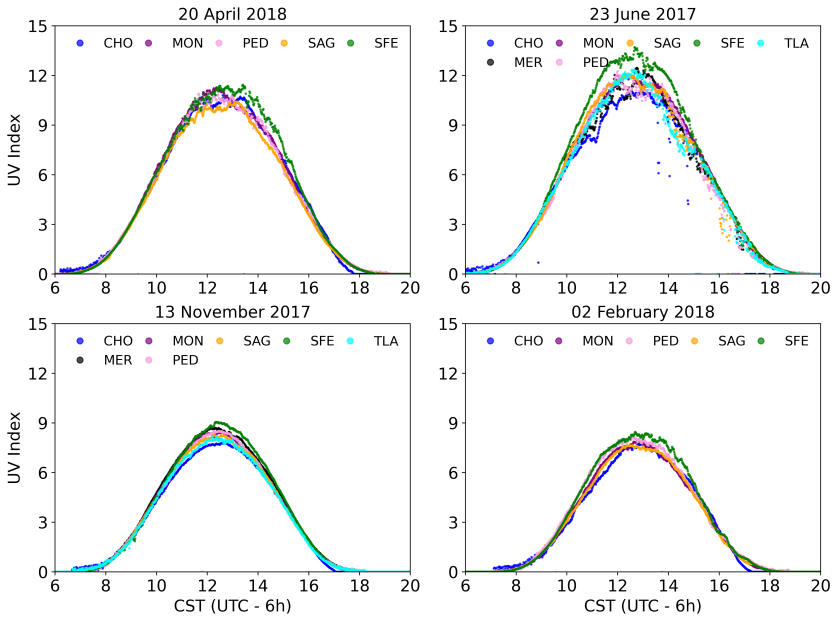

Figure 2: UV Index measured over MCMA by SIMAT stations each minute along the day under practically cloudless conditions for representative days of the year.

The daily maximum UV Index of each station is denoted by $UVI_{\max}$, all of them were counted in the period 2000-2019. As shown in Figure 3, these values ranged from 1 to 16, with a majority (61%) of the days experienced $UVI_{\max}$ values between 6 and 10, and remarkably few, less than 1%, in the higher 13-16 range. The lowest values are likely due to winter days with heavy cloud cover and low sun angles, and UV attenuation by pollutants could also be amplified under such conditions, due to longer photon path lengths at low sun and within clouds. The extreme sparsity of high UVI values remains surprising, and may be an indication of the rarity of extremely unpolluted days within the city.

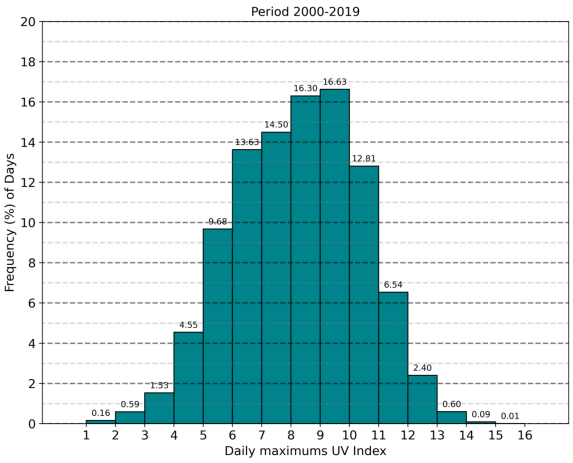

Figure 3: Frequency distribution of daily maximums UV Index values in Mexico City during 2000 -2019.

Similar patterns are found when considering the monthly average of the $UVI_{\max}$ values as shown in Figure 4. The long-term averages present a seasonal variation (as in Fig. 2) that follows approximately the cosine of the noontime solar zenith angle. Notably, values rarely if ever exceed 12 (as in Fig. 3). The lowest average UVI (near 7) take place in winter while from March to August the values seem to be flattened in the range 10-11. The rather low monthly UV Index values, mainly could be a consequence of the presence of clouds in the rainy season. However, urban aerosol pollution sources, biomass burning for agriculture and wood cooking also contribute to poor air quality between March-May[51]. Using the maximum $UVI_{\max}$ from all of stations every day (one daily point), the monthly averages ($\overline{UVI}_m$) were calculated along the period 2000-2019. Long term trends in $\overline{UVI}_m$ are shown in Figure 5. A clear upward trend is seen, with a slope for the linear fit of 0.9%/year or +1.5 UVI units over the two decades.

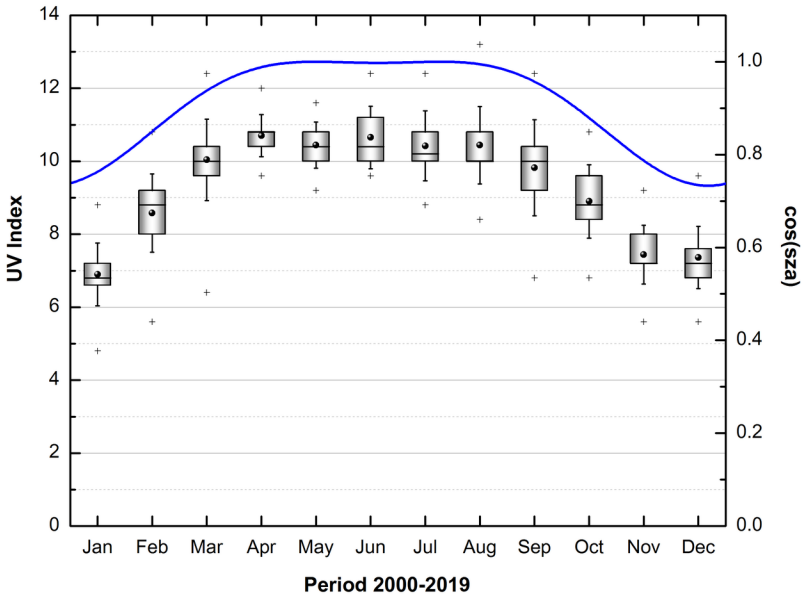

Figure 4: Boxplot of the monthly averages of the maximum UV Index values (black dot) in MCMA for the period 2000-2019: median (central bold line), standard deviation (box edges), 25^{th} and 75^{th} percentiles (the whiskers), the minimum and maximum values (plus sign) and the cosine of the solar zenith angle at solar noon (blue curve).

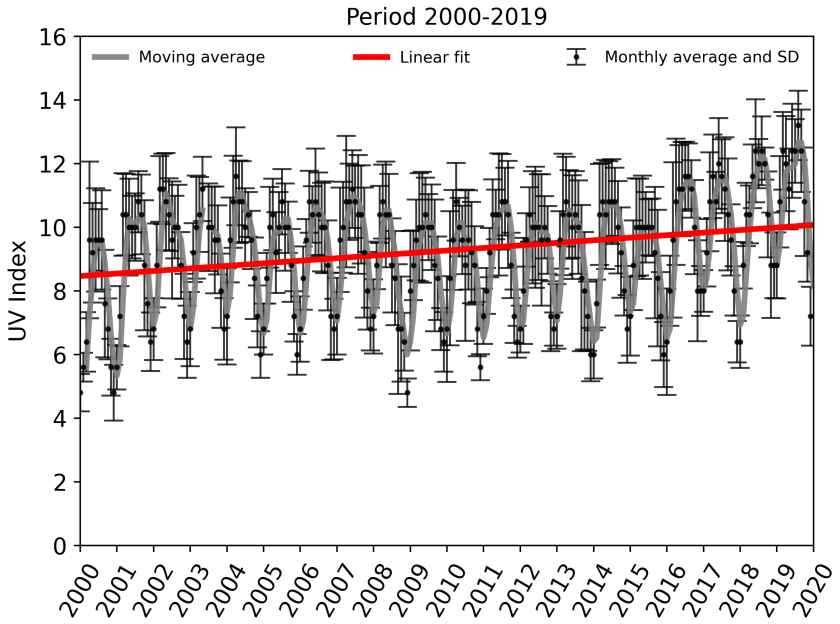

Figure 5: Moving average function (light gray curve) quarterly applied to monthly average UV Index, standard deviation of all data within a given month (black dots and dash line) and linear fit (red line).

The UV Index computed from satellite-based observations (OMI-Aura/NIVR-FMI-NASA) over the period 2005-2019 is mapped in Figure 6. The satellite-derived UVIs vary from 8 in winter to 16 in summer, both values being substantially higher than the ground-based observations (ca. 7 for winter and 11 for summer, see Fig. 4). We hypothesize that this large difference between satellite-based estimation and ground-based observation of the UV index is due to the intense air pollution of Mexico City. A rather similar behavior was detected in Santiago city, Chile.[52]

Close inspection of Figure 6 shows that the maximum values, those from June and July of each year, show a slight but systematic decrease starting ca. 2013. As mentioned in section Methods, this is due to the post-processing of OMI UVI data to account for absorption by BL aerosols[41], using a climatological reduction of about 8% for Mexico City.

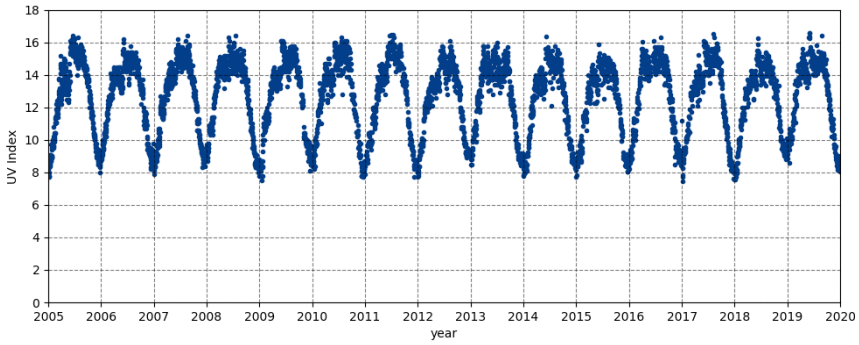

Figure 6: UV Index at solar noon for clear sky recorded by OMI-Aura/NIVR-FMI-NASA, from 2005 to 2019.

Effect of pollutants on UV radiation

Trends and averages in aerosol optical depth AOD_{340} and criteria pollutants PM_{10}, CO, NO_2, O_3 and SO_2 observed at the SIMAT stations over 2000-2019, are shown in Figure 7 and summarized in Table 2 together with the $UVI_{\max}$. Similar trends in pollutants have been noted before[53–55] and reflect the long-term success of emission reduction policies and programs.

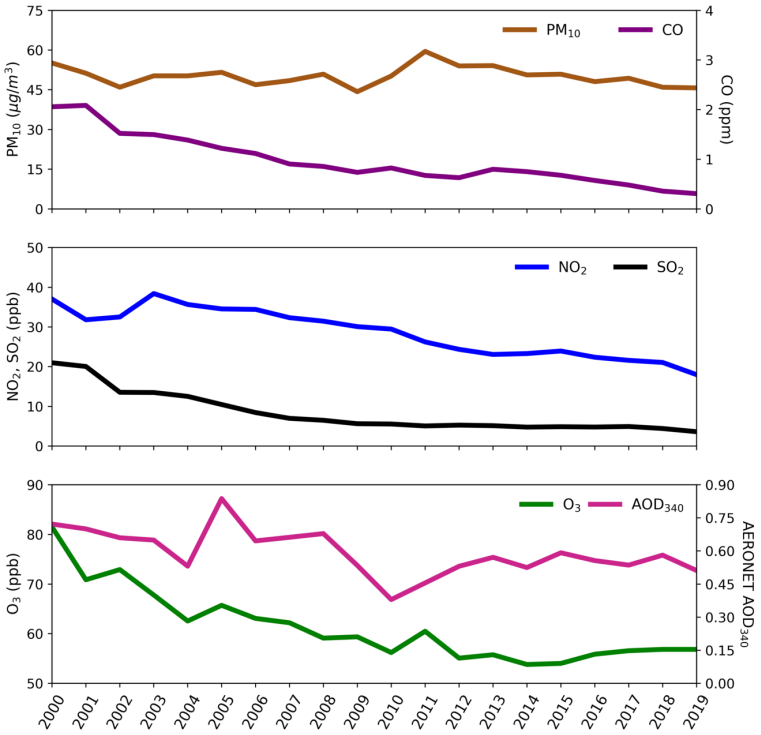

Figure 7: Air quality trends in MCMA for the period 2000-2019 from annual averages obtained between 11h to 15h CST every day: PM_{10} (brown curve), CO (purple curve), NO_2 (blue curve), SO_2(black curve), O_3 (green curve) and AOD_{340} (pink curve).

Table 2: UV Index and criteria pollutants: slope for the period 2000-2019, averages in units of $\mu g/m^3$(PM_{10}), ppm (CO), ppb (SO_2, NO_2 and O_3), dimensionless (UV Index and AOD_{340}) and annual percentage change (%/year).

Variable	$\frac{\Delta variable}{\Delta t}$	$Avg_{2000-2019}$	$\Delta(\%/year)$
UVI	0.08	9.2	0.9
PM_{10}	-0.10	50.2	-0.2
CO	-0.08	1.0	-8.2
NO_2	-0.96	28.6	-3.4
O_3	-1.05	61.3	-1.7
AOD_{340}	-0.01	0.6	-1.6
SO_2	-0.76	8.4	-9.1

The observed changes in the concentrations of these air pollutants have significant implications for surface UV radiation, as can be demonstrated with the TUV radiative transfer model. Table 3 summarizes UVI values for the June-July time period, estimated by the

three methods: OMI satellite-derived UVI, RAMA ground-based observations, and TUV modeling using air pollution estimates. Two groups of values can be readily identified: (1) RAMA daily record values, OMI with or without BL aerosols, and TUV for very clean conditions, all with UVI values around 15-16; and (2) RAMA average daily maxima and TUV UVI using MCMA pollutants as input, which are in good agreement for both 2018/19 and 2000/01 but much lower than the first group. Compared to the OMI estimate that included the climatological aerosol correction (15.3), observed RAMA values were lower by 35% in 2000 and by 20% in 2019. Similarly, TUV values were 35% lower in 2000 and 22% lower in 2019 relative to the TUV values of 15.6 for a pristine atmosphere.

Table 3: UV Index monthly maximum estimates for June-July.

Conditions for estimation in June-July	**UV Index**
RAMA maximum reached in period 2000-2019	15.0
RAMA average maxima 2018, 2019	12.3
RAMA average maxima 2000, 2001	9.9
OMI clear, local noon, no corrected for BL aerosols	16.6
OMI with 8% reduction for BL aerosol (Figure 1 from Arola et al.)	15.3
TUV "zero" pollution AOD 0, O_3 0 ppb, NO_2 0 ppb, SO_2 0 ppb	16.1
TUV pristine pollution AOD 0.05, O_3 10 ppb, NO_2 0 ppb, SO_2 0 ppb	15.6
TUV 2019: AOD 0.5, O_3 50 ppb, NO_2 20 ppb, SO_2 1 ppb	12.1
TUV 2000: AOD 0.7, O_3 70 ppb, NO_2 40 ppb, SO_2 20 ppb	10.2

The agreement between RAMA observations and TUV model estimates is excellent but also probably a bit fortuitous. Clouds on average reduce the irradiance impingent on the surface, but scattering from them can also cause transient enhancements (especially if the direct sunbeam is not blocked) that could be recorded as daily maxima – with cancellation between these cloud effects resulting in improved agreement with the cloud-free model. We cannot exclude that some of the observed trend in UVI is due to changes in cloud cover. However, the modeled fractional UVI reductions due to pollutants, shown in Table 3, are in

such good agreement with the observed UVI reductions, that a compelling case can be made for a dominant role of air pollutants in the long-term UVI trends.

Table 4 shows the contributions to UVI reductions from individual pollutants. Aerosols are seen to be the major factor in both time periods, followed by O_3, NO_2, and SO_2. The 2000-2019 UVI increase is seen to result in comparable proportions from fewer aerosols, less SO_2, and the combined reductions in O_3 and NO_2.

Comparable UV reductions, of 30-40% due to aerosols, were reported by Panicker et al. [11] over Pune, India from April 2004 to March 2005, with sensitivity coefficients (i.e. change in UVI per unit change in AOD) similar to those found here in Table 3.

Comparisons of OMI with ground-based UV measurements have been reviewed recently by Zhang et al. [56] and Vitt et al. [57]. OMI-derived UV generally overestimates ground-level measurements by 1-10% in relatively clean conditions (e.g. rural U.S), by 10-30% in Southern Europe and by 40% or more in Santiago, Chile [52] and Thailand [58]. The overestimations appear related in large part to incomplete accounting of UV absorption by BL aerosol, although other factors such as the correction to solar noon may also introduce some bias. [56] Over Europe, ground-based UVI observations for several decades are systematically lower than those estimated from satellites even after consideration of climatological aerosol distributions, showing the importance of local pollution not resolved from space. [57] However, difference between satellite-derived and ground-based UVI was less than 1.0 UVI units in over 90% of the cases, in contrast to the difference of 3-5 units found for Mexico City (Table 3).

UV reductions by air pollutants are expected to be most severe near the surface, while chemical reactions leading to photochemical smog occur through the vertical extent of the BL. Figure 8 shows the vertical profiles of photolysis coefficients (the reciprocals of photolytic lifetimes) for two key reactions, the photolysis of O_3 to yield excited oxygen atoms O(1D), and the photolysis of NO_2. In the absence of optically active pollutants, these coefficients would be nearly independent of altitude in the BL. However, the presence of pollutants leads to a strong decrease toward the surface, with notably more severe reductions in 2000

compared to 2019. While the specific values shown in the figure are only illustrative for typical conditions, routine daily air quality modeling should carefully account for the long term variations in these photolysis coefficients.

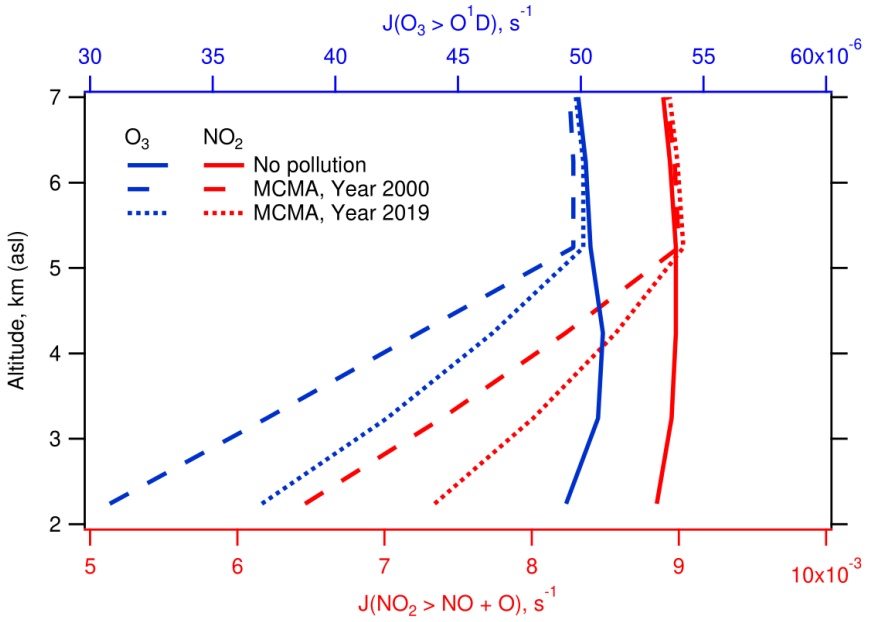

Figure 8: Vertical profiles of the photolysis coefficients for the reaction $O_3+h\nu \rightarrow O(1D)+O_2$ (top axis, blue) $NO_2+h\nu \rightarrow O+NO$ (bottom axis, red) for zero pollution (solid) and Mexico City in the years 2000 (dashed) and 2019 (dotted)

An issue that is beginning to gain relevance in radiative balance models is the influence of a group of organic compounds capable of strongly absorbing in the UV region (brown carbon).[59] Some of these compounds are related with emissions from local and regional wildfires.[60] Mexico City is frequently exposed to regional fire smoke transport during the dry part of the year (November to May)[61], that sporadically modify the optical properties of the aerosols.[62] This could partly explain the relatively minor reductions in PM_{10} (see Fig. 7), compared to the larger reductions of CO, NO_2, and O_3 that are more directly related to urban activities, as well as some of the seasonal asymmetry seen in Fig. 3.

The UVI is specific to wavelengths mainly in the 300-320 nm range, and so the question remains whether these results can be applied at longer UV wavelengths, e.g. those important for NO_2 photolysis (<420 nm). Absorption by SO_2 and O_3 vanishes, while absorption by NO_2

increases and typical aerosols optical depth decrease. These changes can easily be modeled, but unfortunately far fewer measurements of these longer wavelengths are available in Mexico City or elsewhere.

Two decades of observations in Mexico City demonstrate unequivocally that air pollution reduces UV radiation at the ground. The ground-based observations are well below estimates derived from satellite-based observations, and below model calculations do not consider optically important pollutant aerosols, tropospheric ozone, and to a lesser extent NO_2 and SO_2. When typical observed values of these pollutants are included in a model (e.g. TUV), the differences between satellite-derived and ground-based measured values are explained and can be attributed quantitatively to individual observed pollutants. Long term improvements in air quality, over two decades, are accompanied by statistically significant increases in the observed UVI, again in good agreement with the model-predicted changes.

Table 4: Contributions of individual pollutants to UV Index changes. (a) Values used one at the time, with the others held at zero. (b) UVI deviation from the zero-pollution value of 16.1 (from Table 3). (c) 2019-2000 UVI change due to changes in each pollutant.

Pollutant	Year 2000		Year 2019		2019-2000
	poll. level (a)	UVI (b)	poll. level	UVI	(c)
AOD	0.7	-3.7	0.5	-2.7	1.0
O_3 ppb (DU)	70 (14)	-1.4	50 (10)	-1.0	0.4
NO_2 ppb	40	-0.9	20	-0.5	0.4
SO_2 ppb	30	-0.8	1	-0.04	0.8

The reductions in surface UV radiation with respect to an ideally clear atmosphere – by nearly 40% in 2000 and still 20% in 2020 – are large, both within the context of human UV exposure and air quality mitigation. In urban areas where ozone production scales proportionally with UV levels and with volatile organic compound (VOC) emissions (the VOC-limited regime), a 10% increase in BL average photolysis rates means that VOC emissions will need to be reduced by 10% to meet the same goals, or else successful reductions in aerosols would lead to unwanted UV-driven increases in O_3. Such UV changes must be considered carefully in air quality mitigation strategies. For human exposure, a 20% increase in

UV irradiances over two decades should be seen as a non-negligible public health issue requiring some reassessment of preventive behaviors to minimize the risk of skin cancer, cataract, and other UV-related health effects. The efforts that Mexico City has made to improve air quality have achieved positive results in the levels of most air pollutants. Nevertheless, they caused an increase in UV radiation that reaches the surface.

A limitation of the present work is our focus on daily maximum values, which largely exclude cloud cover. Absorption within clouds can be enhanced by the long path lengths of multiply scattered photons (e.g., Mayer et al.[63]), so that accurate quantification of UV effects of clouds in polluted environments remains a significant challenge and interesting opportunity for future work.

Finally, based on our results, the solar radiation monitoring network could be improved by adding observation sites within or close to the basin, with minor influences of the urban plume (e. g., Amecameca; latitude: 19.13^{o}N, longitude: 99.76^{o}W, elevation: 2420 m asl), and the complementing of sensors in existing monitoring sites that are at elevations above the urban boundary layer like Ajusco (AJU, elevation: 2953 m asl) or Instituto de Investigaciones Nucleares (INN, elevation: 3082 m asl). These sites would provide valuable observations to assess quantitatively the effects of urban pollution on solar radiation levels.

Acknowledgement

We wish to acknowledge the staff of SIMAT, from the Secretariat of Environment, for the data and the continuous assistance during the realization of this project. Adriana Ipiña would like to extend her thanks to Dirección General de Personal Académico, Universidad Nacional Autónoma de México (DGAPA-UNAM) for the postdoctoral fellowship at Centro de Ciencias de la Atmósfera of the UNAM. Rubén D Piacentini wishes to thank CONICET and National University of Rosario, Argentina, for their partial support to the present work. The National Center for Atmospheric Research is sponsored by the National Science Foundation.

References

(1) Taylor, H. R.; West, S. K.; Rosenthal, F. S.; Muñoz, B.; Newland, H. S.; Abbey, H.; Emmett, E. A. Effect of Ultraviolet Radiation on Cataract Formation. *New England Journal of Medicine* **1988**, *319*, 1429–1433.

(2) Varotsos, C.; Feretis, E. Health effects on human eye resulting from the increased ambient solar ultraviolet radiation. *Toxicological & Environmental Chemistry* **1997**, *61*, 43–68.

(3) Lucas, R. M.; Yazar, S.; Young, A. R.; Norval, M.; de Gruijl, F. R.; Takizawa, Y.; Rhodes, L. E.; Sinclair, C. A.; Neale, R. E. Human health in relation to exposure to solar ultraviolet radiation under changing stratospheric ozone and climate. *Photochemical & Photobiological Sciences* **2019**, *18*, 641–680.

(4) Leighton, P. A. *Photochemistry of Air Pollution*; Elsevier, 1961; pp v–vi.

(5) Seinfeld, J. H.; Pandis, S. N.; Noone, K. Atmospheric Chemistry and Physics: From Air Pollution to Climate Change. *Physics Today* **1998**, *51*, 88–90.

(6) Finlayson-Pitts, B. J.; Pitts, J. N. *Chemistry of the Upper and Lower Atmosphere*; Academic Press, 2000; pp xvii–xviii.

(7) Liu, S. C.; McKeen, S. A.; Madronich, S. Effect of anthropogenic aerosols on biologically active ultraviolet radiation. *Geophysical Research Letters* **1991**, *18*, 2265–2268.

(8) Sabziparvar, A. A.; Forster, P. M. F.; Shine, K. P. Changes in ultraviolet radiation due to stratospheric and tropospheric ozone changes since preindustrial times. *Journal of Geophysical Research: Atmospheres* **1998**, *103*, 26107–26113.

(9) Madronich, S.; Wagner, M.; Groth, P. Influence of Tropospheric Ozone Control on Exposure to Ultraviolet Radiation at the Surface. *Environmental Science & Technology* **2011**, *45*, 6919–6923.

(10) McKenzie, R. L.; Weinreis, C.; Johnston, P. V.; Liley, B.; Shiona, H.; Kotkamp, M.; Smale, D.; Takegawa, N.; Kondo, Y. Effects of urban pollution on UV spectral irradiances. *Atmospheric Chemistry and Physics* **2008**, *8*, 5683–5697.

(11) Panicker, A. S.; Pandithurai, G.; Takamura, T.; Pinker, R. T. Aerosol effects in the UV-B spectral region over Pune an urban site in India. *Geophysical Research Letters* **2009**, *36*, L10802 1–5.

(12) Palancar, G. G.; Lefer, B. L.; Hall, S. R.; Shaw, W. J.; Corr, C. A.; Herndon, S. C.; Slusser, J. R.; Madronich, S. Effect of aerosols and NO_2 concentration on ultraviolet actinic flux near Mexico City during MILAGRO: measurements and model calculations. *Atmospheric Chemistry and Physics* **2013**, *13*, 1011–1022.

(13) Bais, A. F.; McKenzie, R. L.; Bernhard, G.; Aucamp, P. J.; Ilyas, M.; Madronich, S.; Tourpali, K. Ozone depletion and climate change: impacts on UV radiation. *Photochemical & Photobiological Sciences* **2015**, *14*, 19–52.

(14) Hollaway, M.; Wild, O.; Yang, T.; Sun, Y.; Xu, W.; Xie, C.; Whalley, L.; Slater, E.; Heard, D.; Liu, D. Photochemical impacts of haze pollution in an urban environment. *Atmospheric Chemistry and Physics* **2019**, *19*, 9699–9714.

(15) Li, K.; Jacob, D. J.; Liao, H.; Shen, L.; Zhang, Q.; Bates, K. H. Anthropogenic drivers of 2013–2017 trends in summer surface ozone in China. *Proceedings of the National Academy of Sciences* **2018**, *116*, 422–427.

(16) Wang, Y. et al. *Contrasting trends of PM2.5 and surface-ozone concentrations in China from 2013 to 2017*; Oxford University Press (OUP), 2020; Vol. 7; pp 1331–1339.

(17) Wang, W.; Li, X.; Shao, M.; Hu, M.; Zeng, L.; Wu, Y.; Tan, T. The impact of aerosols on photolysis frequencies and ozone production in Beijing during the 4-year period 2012–2015. *Atmospheric Chemistry and Physics* **2019**, *19*, 9413–9429.

(18) Gao, J.; Li, Y.; Zhu, B.; Hu, B.; Wang, L.; Bao, F. What have we missed when studying the impact of aerosols on surface ozone via changing photolysis rates? *Atmospheric Chemistry and Physics* **2020**, *20*, 10831–10844.

(19) Ma, X.; Huang, J.; Zhao, T.; Liu, C.; Zhao, K.; Xing, J.; Xiao, W. Rapid increase in summer surface ozone over the North China Plain during 2013–2019: a side effect of particulate matters reduction control? *Atmospheric Chemistry and Physics* **2021**, *21*, 1–16.

(20) Bauwens, M.; Compernolle, S.; Stavrakou, T.; Müller, J.-F.; Gent, J.; Eskes, H.; Levelt, P. F.; A, R.; Veefkind, J. P.; Vlietinck, J.; Yu, H.; Zehner, C. Impact of coronavirus outbreak on NO2 pollution assessed using TROPOMI and OMI observations. **2020**, *47*, e2020GL087978.

(21) Venter, Z. S.; Aunan, K.; Chowdhury, S.; Lelieveld, J. COVID-19 lockdowns cause global air pollution declines. *Proceedings of the National Academy of Sciences* **2020**, *117*, 18984–18990.

(22) Shi, X.; Brasseur, G. P. The Response in Air Quality to the Reduction of Chinese Economic Activities During the COVID-19 Outbreak. *Geophysical Research Letters* **2020**, *47*, e2020GL088070.

(23) Le, T.; Wang, Y.; Liu, L.; Yang, J.; Yung, Y. L.; Li, G.; Seinfeld, J. H. Unexpected air pollution with marked emission reductions during the COVID-19 outbreak in China. *Science* **2020**, *369*, 702–706.

(24) Red Automática de Monitoreo Atmosférico (RAMA). http://www.aire.cdmx.gob.mx/descargas/datos/excel/RAMAxls.pdf.

(25) Doran, J. C. et al. The IMADA-AVER Boundary Layer Experiment in the Mexico City Area. *Bulletin of the American Meteorological Society* **1998**, *79*, 2497–2508.

(26) Molina, L. T.; Kolb, C. E.; de Foy, B.; Lamb, B. K.; Brune, W. H.; Jimenez, J. L.; Ramos-Villegas, R.; Sarmiento, J.; Paramo-Figueroa, V. H.; Cardenas, B.; Gutierrez-Avedoy, V.; Molina, M. J. Air quality in North America's most populous city – overview of the MCMA-2003 campaign. *Atmospheric Chemistry and Physics* **2007**, *7*, 2447–2473.

(27) Molina, L. T. et al. An overview of the MILAGRO 2006 Campaign: Mexico City emissions and their transport and transformation. *Atmospheric Chemistry and Physics* **2010**, *10*, 8697–8760.

(28) Jazcilevich, A. D.; García, A. R.; Caetano, E. Locally induced surface air confluence by complex terrain and its effects on air pollution in the valley of Mexico. *Atmospheric Environment* **2005**, *39*, 5481–5489.

(29) Tie, X.; Madronich, S.; Li, G.; Ying, Z.; Zhang, R.; Garcia, A. R.; Lee-Taylor, J.; Liu, Y. Characterizations of chemical oxidants in Mexico City: A regional chemical dynamical model (WRF-Chem) study. *Atmospheric Environment* **2007**, *41*, 1989–2008.

(30) Zhang, Y.; Dubey, M. K.; Olsen, S. C.; Zheng, J.; Zhang, R. Comparisons of WRF/Chem simulations in Mexico City with ground-based RAMA measurements during the 2006-MILAGRO. *Atmospheric Chemistry and Physics* **2009**, *9*, 3777–3798.

(31) Zavala, M.; Brune, W. H.; Velasco, E.; Retama, A.; Cruz-Alavez, L. A.; Molina, L. T. Changes in ozone production and VOC reactivity in the atmosphere of the Mexico City Metropolitan Area. *Atmospheric Environment* **2020**, *238*, 117747.

(32) WHO,; WMO,; UNEP,; ICNIRP, *Global solar UV index : a practical guide*; 2002; pp A joint recommendation of the World Health Organization, World Meteorological Organization, United Nations Environment Programme, and the International Commission on Non–Ionizing Radiation Protection.

(33) Webb, A. R.; Slaper, H.; Koepke, P.; Schmalwieser, A. W. Know Your Standard: Clari-

fying the CIE Erythema Action Spectrum. *Photochemistry and Photobiology* **2011**, *87*, 483–486.

(34) Whiteman, C. D.; Zhong, S.; Bian, X.; Fast, J. D.; Doran, J. C. Boundary layer evolution and regional-scale diurnal circulations over the and Mexican plateau. *Journal of Geophysical Research: Atmospheres* **2000**, *105*, 10081–10102.

(35) Fast, J. D.; de Foy, B.; Rosas, F. A.; Caetano, E.; Carmichael, G.; Emmons, L.; McKenna, D.; Mena, M.; Skamarock, W.; Tie, X.; Coulter, R. L.; Barnard, J. C.; Wiedinmyer, C.; Madronich, S. A meteorological overview of the MILAGRO field campaigns. *Atmospheric Chemistry and Physics* **2007**, *7*, 2233–2257.

(36) Carreón-Sierra, S.; Salcido, A.; Castro, T.; Celada-Murillo, A.-T. Cluster Analysis of the Wind Events and Seasonal Wind Circulation Patterns in the Mexico City Region. *Atmosphere* **2015**, *6*, 1006–1031.

(37) Sistema de Monitoreo Atmosférico (SIMAT). www.aire.cdmx.gob.mx, www.aire.cdmx.gob.mx/default.php.

(38) Holben, B.; Eck, T.; Slutsker, I.; Tanré, D.; Buis, J.; Setzer, A.; Vermote, E.; Reagan, J.; Kaufman, Y.; Nakajima, T.; Lavenu, F.; Jankowiak, I.; Smirnov, A. AERONET—A Federated Instrument Network and Data Archive for Aerosol Characterization. *Remote Sensing of Environment* **1998**, *66*, 1–16.

(39) Carabali, G.; Estévez, H. R.; Valdés-Barrón, M.; Bonifaz-Alfonzo, R.; Riveros-Rosas, D.; Velasco-Herrera, V. M.; Vázquez-Gálvez, F. A. Aerosol climatology over the Mexico City basin: Characterization of optical properties. *Atmospheric Research* **2017**, *194*, 190–201.

(40) NASA EOS/Aura Validation Data Center (AVDC) - Correlative data, Field of View Predictions, Data Subsets, GEOMS, DCIO. https://avdc.gsfc.nasa.gov/pub/most_popular/overpass/OMI/.

(41) Arola, A. et al. A new approach to correct for absorbing aerosols in OMI UV. *Geophysical Research Letters* **2009**, *36*, L22805 1–5.

(42) Madronich, S. Intercomparison of NO2 photodissociation and U.V. Radiometer Measurements. *Atmospheric Environment* **1987**, *21*, 569–578.

(43) Shaw, W. J.; Pekour, M. S.; Coulter, R. L.; Martin, T. J.; Walters, J. T. The daytime mixing layer observed by radiosonde profiler, and lidar during MILAGRO. *Atmospheric Chemistry and Physics Discussions* **2007**, *7*, 15025–15065.

(44) Velasco, E.; Márquez, C.; Bueno, E.; Bernabé, R. M.; Sánchez, A.; Fentanes, O.; Wöhrnschimmel, H.; Cárdenas, B.; Kamilla, A.; Wakamatsu, S.; Molina, L. T. Vertical distribution of ozone and VOCs in the low boundary layer of Mexico City. *Atmospheric Chemistry and Physics* **2008**, *8*, 3061–3079.

(45) Greenberg, J.; Guenther, A.; Turnipseed, A. Tethered balloon-based soundings of ozone aerosols, and solar radiation near Mexico City during MIRAGE-MEX. *Atmospheric Environment* **2009**, *43*, 2672–2677.

(46) Rogers, R. R.; Hair, J. W.; Hostetler, C. A.; Ferrare, R. A.; Obland, M. D.; Cook, A. L.; Harper, D. B.; Burton, S. P.; Shinozuka, Y.; McNaughton, C. S.; Clarke, A. D.; Redemann, J.; Russell, P. B.; Livingston, J. M.; Kleinman, L. I. NASA LaRC airborne high spectral resolution lidar aerosol measurements during MILAGRO: observations and validation. *Atmospheric Chemistry and Physics* **2009**, *9*, 4811–4826.

(47) Lewandowski, P. A.; Eichinger, W. E.; Holder, H.; Prueger, J.; Wang, J.; Kleinman, L. I. Vertical distribution of aerosols in the vicinity of Mexico City during MILAGRO-2006 Campaign. *Atmospheric Chemistry and Physics* **2010**, *10*, 1017–1030.

(48) Corr, C. A.; Krotkov, N.; Madronich, S.; Slusser, J. R.; Holben, B.; Gao, W.; Flynn, J.; Lefer, B.; Kreidenweis, S. M. Retrieval of aerosol single scattering albedo at ultraviolet

wavelengths at the T1 site during MILAGRO. *Atmospheric Chemistry and Physics* **2009**, *9*, 5813–5827.

(49) Castro, T.; Madronich, S.; Rivale, S.; Muhlia, A.; Mar, B. The influence of aerosols on photochemical smog in Mexico City. *Atmospheric Environment* **2001**, *35*, 1765–1772.

(50) SEDEMA, *Calidad del aire en la Ciudad de México, Informe 2017*; 2018.

(51) Retama, A.; Baumgardner, D.; Raga, G. B.; McMeeking, G. R.; Walker, J. W. Seasonal and diurnal trends in black carbon properties and co-pollutants in Mexico City. *Atmospheric Chemistry and Physics* **2015**, *15*, 9693–9709.

(52) Cabrera, S.; Ipiña, A.; Damiani, A.; Cordero, R. R.; Piacentini, R. D. UV index values and trends in Santiago Chile (33.5°S) based on ground and satellite data. *Journal of Photochemistry and Photobiology B: Biology* **2012**, *115*, 73–84.

(53) Parrish, D. D.; Singh, H. B.; Molina, L.; Madronich, S. Air quality progress in North American megacities: A review. *Atmospheric Environment* **2011**, *45*, 7015–7025.

(54) Secretaría del Medio Ambiente de la Ciudad de México, *Calidad del aire en la Ciudad de México, informe 2017*; 2018; pp 1–160.

(55) Molina,; Velasco,; Retama,; Zavala, Experience from Integrated Air Quality Management in the Mexico City Metropolitan Area and Singapore. *Atmosphere* **2019**, *10*, 512.

(56) Zhang, H.; Wang, J.; García, L. C.; Zeng, J.; Dennhardt, C.; Liu, Y.; Krotkov, N. A. Surface erythemal UV irradiance in the continental United States derived from ground-based and OMI observations: quality assessment trend analysis and sampling issues. *Atmospheric Chemistry and Physics* **2019**, *19*, 2165–2181.

(57) Vitt, R.; Laschewski, G.; Bais, A.; Diémoz, H.; Fountoulakis, I.; Siani, A.-M.;

Matzarakis, A. UV-Index Climatology for Europe Based on Satellite Data. *Atmosphere* **2020**, *11*, 727.

(58) Janjai, S.; Wisitsirikun, S.; Buntoung, S.; Pattarapanitchai, S.; Wattan, R.; Masiri, I.; Bhattarai, B. K. Comparison of UV index from Ozone Monitoring Instrument (OMI) with multi-channel filter radiometers at four sites in the tropics: effects of aerosols and clouds. *International Journal of Climatology* **2013**, *34*, 453–461.

(59) Laskin, A.; Laskin, J.; Nizkorodov, S. A. Chemistry of Atmospheric Brown Carbon. *Chemical Reviews* **2015**, *115*, 4335–4382.

(60) Gadhavi, H.; Jayaraman, A. Absorbing aerosols: contribution of biomass burning and implications for radiative forcing. *Annales Geophysicae* **2010**, *28*, 103–111.

(61) Rios, B.; Raga, G. B. Smoke emissions from agricultural fires in Mexico and Central America. *Journal of Applied Remote Sensing* **2019**, *13*, 1.

(62) Barnard, J. C.; Volkamer, R.; Kassianov, E. I. Estimation of the mass absorption cross section of the organic carbon component of aerosols in the Mexico City Metropolitan Area. *Atmospheric Chemistry and Physics* **2008**, *8*, 6665–6679.

(63) Mayer, B.; Kylling, A.; Madronich, S.; Seckmeyer, G. Enhanced absorption of UV radiation due to multiple scattering in clouds: Experimental evidence and theoretical explanation. *Journal of Geophysical Research: Atmospheres* **1998**, *103*, 31241–31254.

Graphical TOC Entry

Some journals require a graphical entry for the Table of Contents. This should be laid out "print ready" so that the sizing of the text is correct.

Inside the `tocentry` environment, the font used is Helvetica 8 pt, as required by *Journal of the American Chemical Society*.

The surrounding frame is 9 cm by 3.5 cm, which is the maximum permitted for *Journal of the American Chemical Society* graphical table of content entries. The box will not resize if the content is too big: instead it will overflow the edge of the box.

This box and the associated title will always be printed on a separate page at the end of the document.